Huang, Tianbai; Kupfer, Stephan; Richter, Martin; Gräfe, Stefanie; Geitner, Robert

Bidentate Rh(I)-phosphine complexes for the C-H activation of alkanes: computational modelling and mechanistic insight

Original published in:	ChemCatChem. - Weinheim : WILEY-VCH Verlag. - 14 (2022), 18, art. e202200854, 9 pp.
Original published:	2022-07-22
ISSN:	1867-3899 ; 1867-3880
DOI:	10.1002/cctc.202200854
[*Visited:*	2023-01-31]

ChemCatChem

Research Article
doi.org/10.1002/cctc.202200854

Chemistry Europe
European Chemical Societies Publishing

www.chemcatchem.org

Bidentate Rh(I)-Phosphine Complexes for the C–H Activation of Alkanes: Computational Modelling and Mechanistic Insight

Tianbai Huang,[a] Stephan Kupfer,[a] Martin Richter,[a, b] Stefanie Gräfe,[a] and Robert Geitner*[c]

The C–H activation and subsequent carbonylation mediated by metal complexes, i.e., Rh(I) complexes, has drawn considerable attention in the past. To extend the mechanistic insight from Rh complexes featuring monodentate ligands like $P(Me)_3$ towards more active bisphosphines (PLP), a computationally derived fully conclusive mechanistic picture of the Rh(I)-catalyzed C–H activation and carbonylation is presented here. Depending on the nature of the bisphosphine ligand, the highest lying transition state (TS) is associated either to the initial C–H activation in [Rh(PLP)(CO)(Cl)] or to the rearrangement of the chloride in [Rh(PLP)(H)(R)(Cl)]. The chloride rearrangement was found to play a key role in the subsequent carbonylation. A set of 20 complexes of different architectures was studied, in order to fine tune the C–H activation in a knowledge-driven approach. The computational analysis suggests that a flexible ligand architecture with aromatic rings can potentially increase the performance of Rh-based catalysts for the C–H activation.

Introduction

Petroleum is the foundation of the chemical industry, as it provides the most important raw chemicals in synthetic chemistry – alkenes, which are mainly produced via catalytic cracking[1] from alkanes, one of the main constituents of crude oil. Compared to alkenes with a C=C double bond accessible for chemical functionalization, alkanes are chemically more stable under most conditions due to the inert nature of the C–H (as well as of the C–C) bonds, and hence are hardly convertible into other more valuable functionalized compounds, e.g., aldehydes, alcohols,[2] or cyanides.[3]

However, in comparison to the catalytic cracking process, the direct transformation of alkanes into other compounds benefits from the high atom efficiency as well as the lower number of conversion steps. Key to the conversion of alkanes is the activation of the inert C–H bond. Currently, four distinct reaction mechanisms are known to realize C–H bond activation,[4] namely oxidative addition,[5] σ-bond metathesis,[6] electrophilic substitution (amphiphilic metal ligand activation)[7] and base-assisted metalation.[8] Among these mechanisms, oxidative addition using electron-rich transition metal complexes, e.g., based on Rh(I), has drawn most attention in the field of C–H activation due to its versatility.[5–9]

The broad range of applications of organometallic compounds in catalytic processes originates from their favorable redox properties, which can be easily tuned and optimized to the specific chemical process of interest by alteration of the metal center but even more importantly, by structural modification of the ligand sphere. With respect to the oxidative addition reaction, the addition of strongly coordinating σ-donor ligands such as phosphines,[10] N-heterocyclic carbenes[11] or bidentate nitrogen-containing molecules,[12] can be beneficial to enhance the chemical stability and, thus, the long-term performance of the molecular catalyst, as well as to provide a handle for tuning the oxidation potential of the metal center, and in consequence, the catalytic turnover.[13] Sawamura et al.[14] discovered that the yields of Rh-catalyzed borylation with assisting phosphine ligand increased by approximately 10% compared to phosphine-free conditions. Furthermore, Semproni et al.[15] found that introducing an electron-donating ^{iPr}PNP ligand enabled the oxidative addition of H_2 or of C–H bonds in benzene onto the central Co(I). From the classes of the mentioned ligands, bidentate and polydentate phosphine ligands are among the most promising ligands in C–H activation, due to the chelate effect[16] as well as due to the strong σ-donor strength induced by the phosphor atoms.[17] Despite the extensive number of experimental investigations on the transition metal-mediated C–H activation,[9b,18] there is still a lack of insight with respect to the underlying reaction mechanism at the molecular level when dealing with alkanes. In this regard, Sakakura et al.[5] postulated a mechanism for the C–H carbonylation of alkanes using Rh(I)-complexes with

[a] T. Huang, Dr. S. Kupfer, Dr. M. Richter, Prof. S. Gräfe
Institute for Physical Chemistry (IPC) and Abbe Center of Photonics
Friedrich Schiller University Jena
Helmholtzweg 4, 07743 Jena (Germany)
[b] Dr. M. Richter
Present address:
DS Deutschland GmbH
Am Kabellager 11–13, 51063 Cologne (Germany)
[c] Prof. R. Geitner
Institute of Chemistry and Bioengineering
Technical University Ilmenau
Weimarer Str. 32, 98693 Ilmenau (Germany)
E-mail: robert.geitner@tu-ilmenau.de

Supporting information for this article is available on the WWW under https://doi.org/10.1002/cctc.202200854

monodentate phosphine ligands. Bridgewater et al.[19] performed time-resolved optical (TRO) spectral and nanosecond time-resolved infrared (TRIR) spectral studies onto *trans*-[Rh-(P_2)(CO)(Cl)] complexes, which provides a strong evidence for the light-induced CO loss. Furthermore, several experimental results also confirmed the importance of the light-drivenCO loss in the C–H activation step catalyzed by Rh-based complexes featuring Cp (η^5-C_5H_5) ligands[1b,20] or Tp* (HB–Pz*$_3$, Pz* = 3,5-dimethylpyrazolyl) ligands.[9b,21] Unfortunately, the scope of the full description of the mechanism of the investigated phosphines was limited exclusively to monodentate PR_3 ligands. Thus, the mechanistic insight obtained for the highly flexible monodentate ligand sphere, is not fully applicable to the case of more rigid bidentate ligands.

The present computational study aims to build on the previously obtained knowledge while extending the mechanistic insight in the frame of transition metal complex-mediated C–H activation in alkanes to the family of bidentate phosphine ligands. In particular, we focused on the C–H carbonylation of the terminal carbon of propane by Rh(I)-complexes featuring various bidentate phosphine ligands (PLP), see Figure 1, and derived the underlying reaction mechanism based on the catalytic intermediates along several reaction pathways.

To this aim, we applied quantum chemical simulations at the density functional level of theory (DFT) to investigate the electronic properties of catalytic intermediates featuring the mentioned ligands, which cover a broad range of ligand structures. Based on the results of the mechanistic investigation, we strive to improve the catalytic performance of present C–H catalysts by virtue of a knowledge-driven approach, which correlates structural features to catalytic performance.

Results and Discussions

Bidentate ligand selection

In this mechanistic study, we focused on 20 prototypic PLP ligands to evaluate structure-property dependencies in the catalytic C–H activation of propane (see Figure 1). During an initial screening process on the computational calculation process, we furthermore excluded the ligands with a flexible linker consisting of more than four atoms, namely ligands **7**, **10**, **18** and **20**, because flexible linkers enable cis-trans conformational change during the reaction, which increases the complexity of determining the reaction path significantly. Typically, the active species for C–H activation [Rh(PLP)(Cl)] is generated from

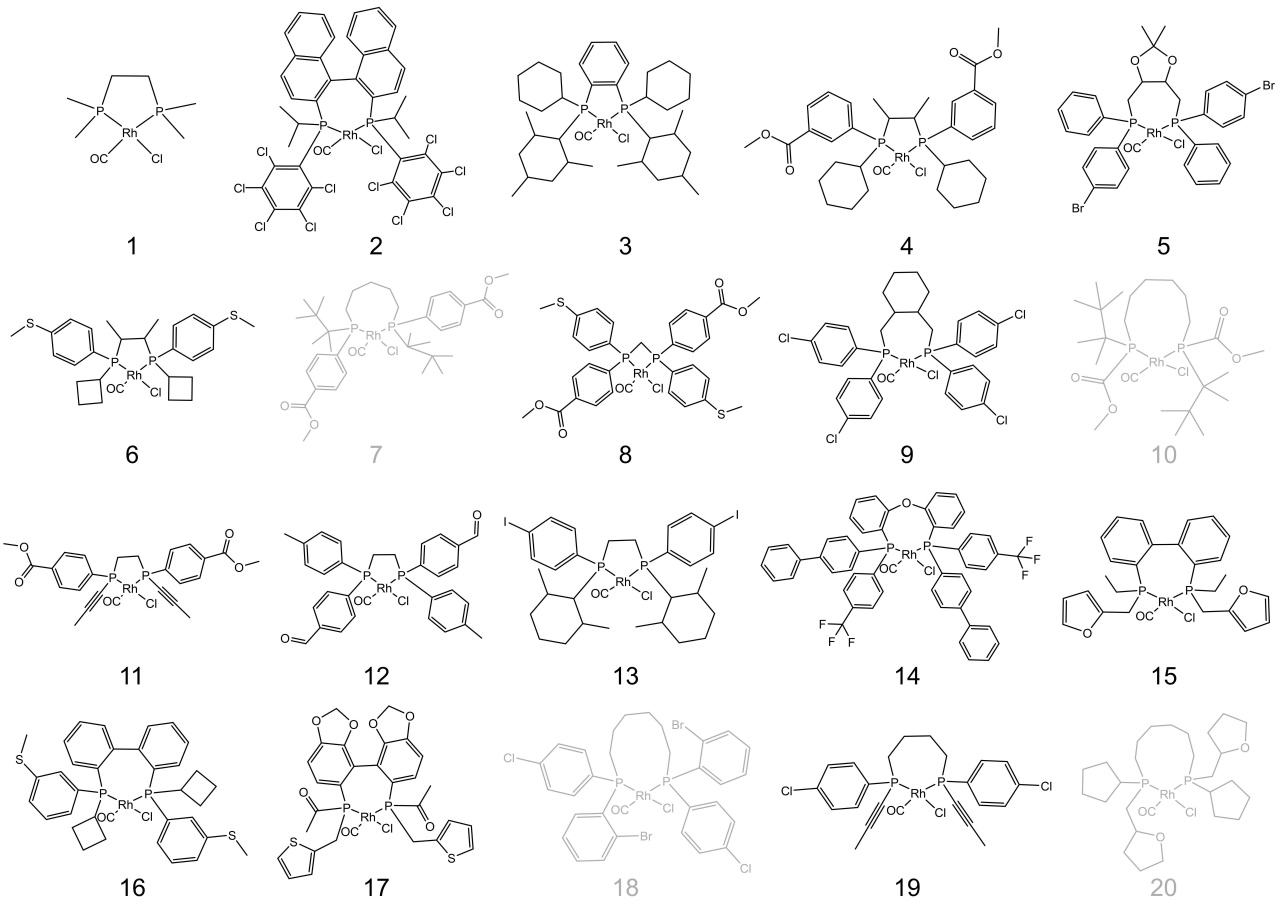

Figure 1. Structures of investigated Rh(I) complexes with bidentate phosphine ligands in the scope of C–H activation (i.e. propane). In-depth quantum chemical studies were performed for all systems in black while species in grey are omitted from mechanistic studies as they feature low-lying triplet states.

the precursor [Rh(PLP)(CO)(Cl)] via a light-driven CO elimination. This activation process is not studied in-depth in this investigation, which focuses on the subsequent reaction pathways. However, to evaluate the impact of (long-lived) triplet states, which are potentially accessible upon intersystem-crossing, on the reaction steps of the C–H activation, we carefully analyzed the energetics of the low-lying spin states in all 20 Rh phosphine complexes. In all cases, the closed-shell (singlet) configuration was thermodynamically more favorable than the open-shell (triplet) species (see Table S3 for details). However, it is also observed that complexes featuring ligand **7**, **10**, **18** and **20** were predicted to have a smaller singlet-triplet energy gap than the others. Noteworthy, the stabilization of the high-spin state is likely associated with the flexible nature of these ligands (see above), which allows a rapid alternation of the coordination sphere upon light-driven CO dissociation. Thus, we focused our theoretical investigations with respect to further mechanistic insights on the remaining 16 complexes.

Mechanistic model

Based on the mechanism regarding the carbonylation of alkanes using monodentate phosphine ligands proposed by Sakakura et al.,[5] we suggest a refined, computationally derived mechanism for C–H carbonylation using [Rh(PLP)(CO)(Cl)] complexes, Figure 2. As for the previously proposed mechanism,[5] our catalytic cycle also starts from a stable square-planar species I'. Thereafter, the catalyst is activated by the light-induced CO loss, which generates a highly active triply coordinated Rh(I) species I. This light-driven step does not only raise the catalyst to a high energy level, but also creates a spatially accessible vacancy for the alkane (propane as model compound in this study), which allows the subsequent oxidative addition (I→II). Thereafter, the chloride ion rotates in the newly formed square-pyramidal complex II to form III, which leads to a vacancy in the equatorial plane. This transformation is followed by the addition of a CO molecule to complex III forming the octahedral carbonyl complex IV. Subsequently, the CO molecule inserts into the Rh–C bond of the propyl group, forming an acyl complex (IV→V). This reaction again generates a vacancy, which enables the addition of a second CO molecule, forming the stable octahedral complex VI with an 18-electron configuration. In the last step (VI→VII), the product, here butyraldehyde, is formed via reductive elimination and the associated cleavage of the Rh–H and Rh–C bonds. Consequently, the initial square-planar Rh complex is regenerated closing the catalytic cycle.

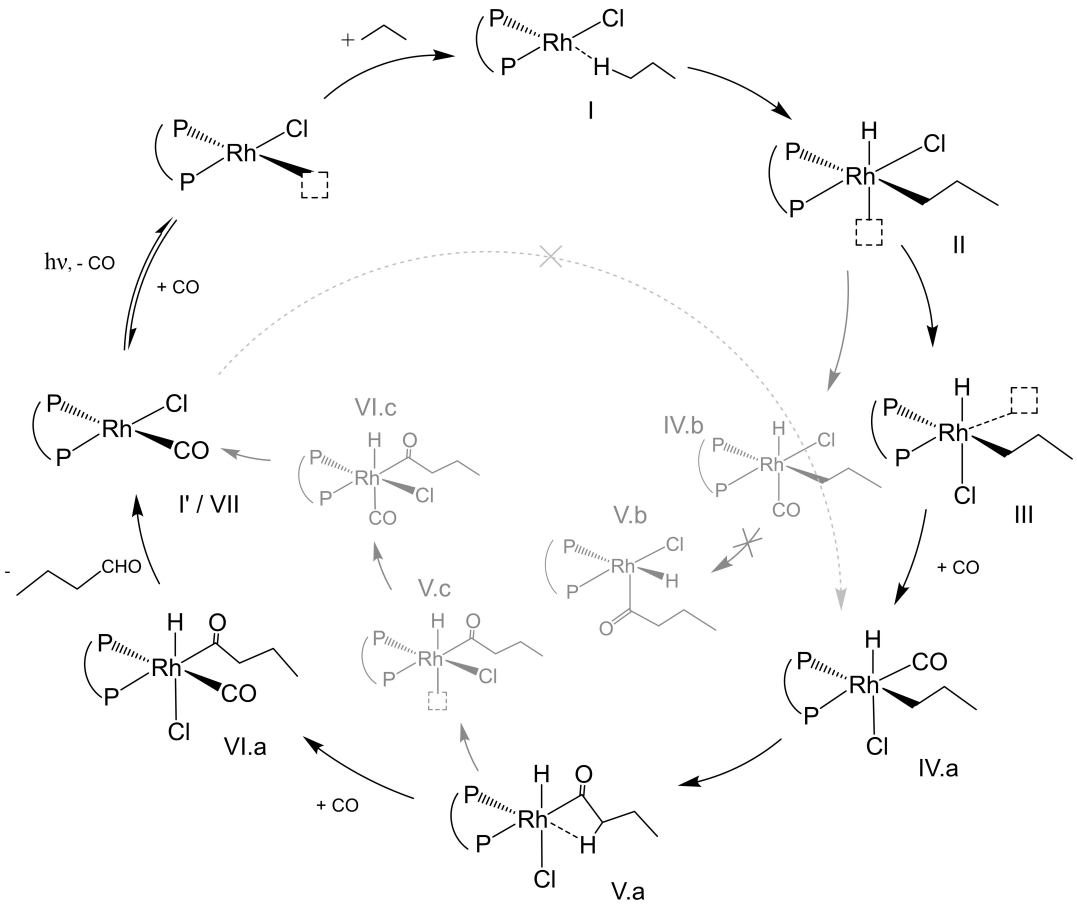

Figure 2. Schematic representation of C–H functionalization mechanism. Structures in black represent main intermediates along the reaction while those in grey are possible side intermediates for the reaction. Paths with crosses are potentially inaccessible due to high activation barriers.

Reaction profile

The corresponding energy profile of the entire catalytic cycle for complex 1 is shown in Figure 3. All steps labelled by roman numbers denote (local) minima on the potential energy (hyper-)surface (PES), namely the educt, intermediates and product. Further, the energy levels of transition states (TSs) connecting the respective minima are also indicated in the profile. Comparing the energy level of I' and I, it is apparent that the initial light-activation provides a substantial amount of energy acting as the driving force for the entire catalytic cycle. As evident from the energy landscape predicted on the level of density functional theory (DFT, see Computational Section for details), three noticeably high barriers could hamper the overall catalytic turnover frequency (TOF): This includes the C–H oxidative addition (I→II, 94.63 kJ mol^{-1}), the C–C bond formation (IV→V, 66.98 kJ mol^{-1}) as well as the reductive elimination of butyraldehyde (VI→VII, 82.24 kJ mol^{-1}). On the other hand, both CO addition steps (III→IV and V→VI) are barrierless and stabilize the system significantly. From this point of view, the C–H addition could be the rate-determining step of the entire catalytic cycle. However, according to the energetic span model,[22] the TOF of a catalyst is not determined by the difference between the TS and the intermediate within the same elementary reaction, but is dependent on the largest energy gap between the TS and the intermediate in the entire catalytic cycle, namely the apparent activation energy δE. The relation is described by Equation (1):

$$\mathrm{TOF} = \frac{k_B T}{h} e^{-\delta E/RT}, \tag{1}$$

where the apparent activation energy is determined by the turnover-determining transition state (TDTS) and turnover-determining intermediate (TDI), both of which could be termed as the rate determining states of the catalytic cycles [Equation (2)].

$$\delta E = \begin{cases} G_{TDTS} - G_{TDI} & \textit{TDTS after TDI}, \\ G_{TDTS} - G_{TDI} + \Delta G_r & \textit{TDTS before TDI}. \end{cases} \tag{2}$$

Due to the high energy of the five-times coordinated structure (II), obtained upon C–H activation, the TS associated with Cl rotation (II→III) could also be a competitor for the TDTS depending on the structure of the utilized ligand, although the step itself requires only 15.62 kJ mol^{-1} to overcome in the case of complex **1**. Based on the energetic span model [Equation (1)], the TOF of Rh-catalysts featuring different ligands, approximated by the energy levels of two competing TSs and the corresponding apparent activation energy, are summarized in Table 1. From the table it can be concluded that complex **9** is predicted to have the highest TOF with δE being approximately 80 kJ mol^{-1}. On the one hand, complexes **6**, **8** and **14** feature ligands with electron-donating phenyl groups which results in a low barrier of the C–H activation (I→II). On the other hand, except for the complexes featuring bulky ligands, e.g., **2** and **14**, the activation barrier for the subsequent rearrangement is

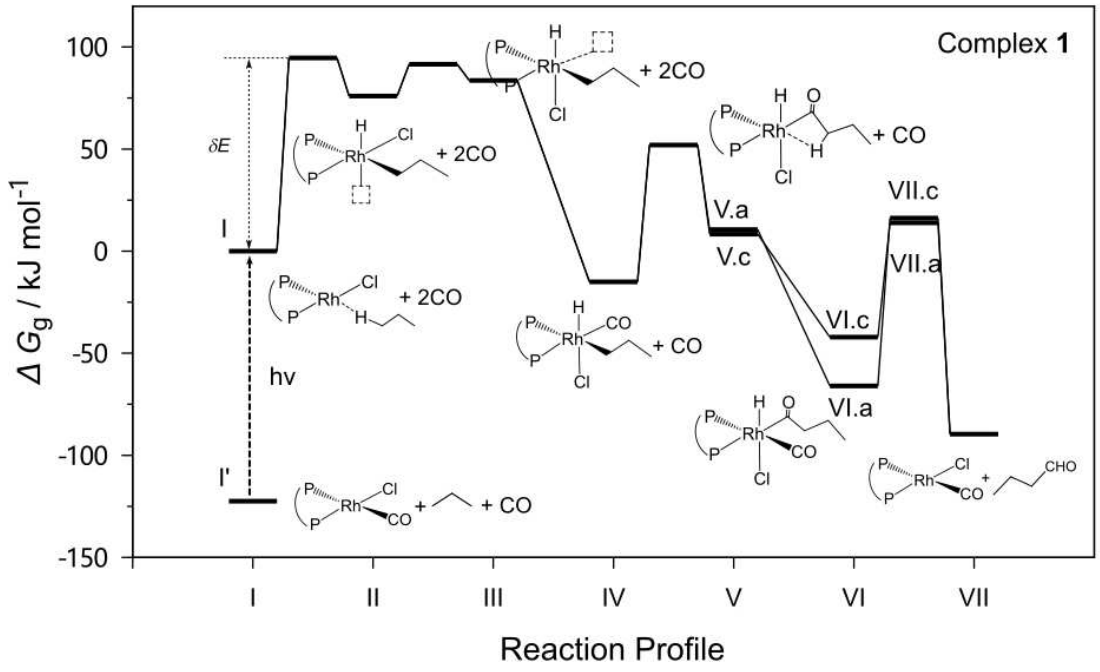

Figure 3. DFT-predicted reaction profile of the mechanism, shown exemplarily for complex **1**. All energies are shown with respect to intermediate I, obtained upon photo-activation of I'. The corresponding elementary steps are labeled as followed: I→II: C–H (oxidative) addition; II→III: Cl rotation; III→IV: CO insertion; IV→V C–C formation; V→VI: CO insertion; VI→VII: butyraldehyde generation, see Figure 2 for reaction details). For clarity, structures of intermediates are provided.

Table 1. Approximated turnover frequencies [TOF in s^{-1}, according to Equation (1)] at 298.15 K, energy level ($\Delta G_g(TS_i)$ in kJ mol^{-1}) of TS associated to C–H activation (I→II) and chloride rearrangement (II→III) as well as the barrier height (E_a in kJ mol^{-1}) between II and III of Rh-complexes featuring different ligands. The apparent activation energy δE of the catalytic cycle is highlighted in bold.

Complex	TOF	ΔG_g [$TS_{I\rightarrow II}$]	ΔG_g [$TS_{II\rightarrow III}$]	E_a [$TS_{II\rightarrow III}$]
1	1.64×10^{-4}	**95**	92	16
2	1.20×10^{-11}	105	**135**	55
3	1.01×10^{-6}	96	**107**	27
4	5.23×10^{-6}	101	**103**	27
5	7.05×10^{-5}	**97**	85	15
6	4.39×10^{-4}	**92**	89	15
8	4.65×10^{-3}	**86**	70	8
9	7.05×10^{-2}	**80**	72	15
11	1.46×10^{-4}	94	**95**	7
12	1.30×10^{-8}	96	**118**	32
13	5.20×10^{-8}	**115**	101	4
14	1.67×10^{-4}	86	**95**	45
15	9.02×10^{-6}	93	**102**	33
16	3.81×10^{-5}	**98**	97	5
17	2.17×10^{-5}	**100**	91	8
19	8.81×10^{-9}	**119**	102	7

relatively low. This leads to complex **9** having the highest TOF. From this data, we can preliminarily conclude that the catalytic performance could benefit from a less-bulky ligand with electron-donating character. However, an in-depth correlation between the ligand structures and the resulting energy states requires more data, which is part of future studies.

Influence of ligand structure

With the general mechanism in mind, this section describes structure-property dependencies and alternative pathways found for the individual elementary steps.

C–H addition

Figure 4a describes the energetic properties of the TSs and intermediates of the two possible pathways of the C–H addition (I→II vs. I'→IV) for various ligands. Based on this substantial difference in activation energy, it becomes clear that the initial

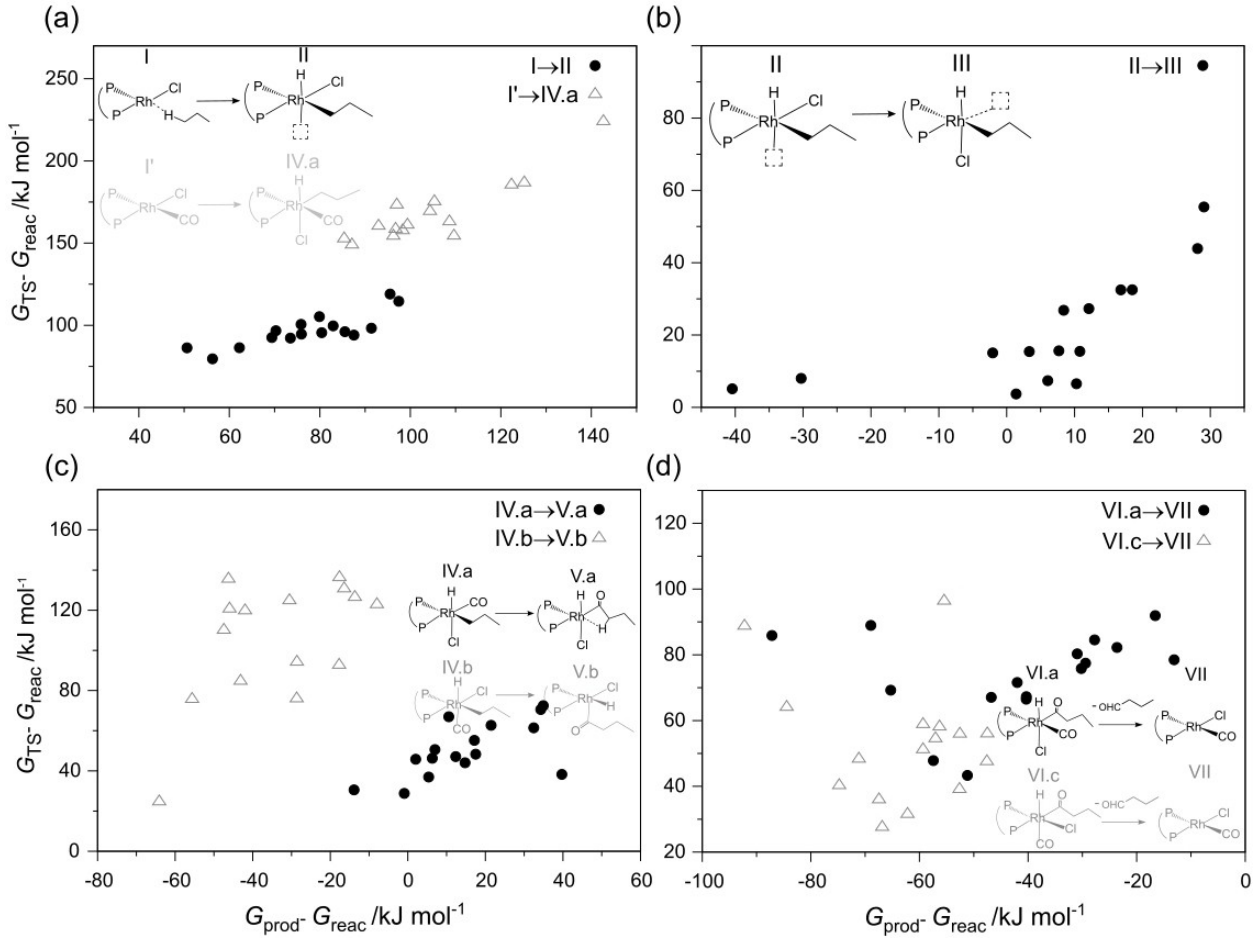

Figure 4. Performance (driving force vs. activation barrier) of different ligands on selected key elementary reactions in the catalytic cycle: (a) C–H addition (I→II), (b) Cl rotation (II→III), (c) C–C formation (IV→V) and (d) butyraldehyde formation (VI→VII). Data points represented by black dots (●) describe the driving force and corresponding activation energy of the main reaction pathway of the corresponding steps, while the hollow grey triangles (△) describe possible alternative pathways, respectively. For details, please refer to the main text.

light-induced CO loss in I→II considerably reduces the barrier height of the C–H activation when compared to the direct activation in I'→IV. This is important as the $TS_{I\rightarrow II}$ could potentially be the rate-determining state of the entire reaction (Table 1). The reason of the lower activation barrier for the path from I→II is twofold: Firstly, compared to the mechanism that starts with the four-times coordinated structure I', the generation of a vacancy in I avoids the rotation of other ligands to the axial position during the C–H activation reaction. Secondly, a strong attractive interaction between the subsequently activated hydrogen atom and the central Rh ion is formed due to the vacancy in I. This pre-coordination reduces the activation barrier for the C–H activation substantially.

The attractive interaction can be visualized by an interaction region indicator (IRI) analysis.[23] Similar to the reduced density gradient (RDG) analysis[24] that can be performed via NCIPLOT,[25] the IRI function also utilizes the information of the electron density of the molecular system and its gradient, however, is better parametrized. The value of an IRI function is small in the region of chemical bonds as well as in case of weak interactions, compared to the value in the vicinity of nuclei and at the edge of molecules. Hence, these interaction regions could be clearly distinguished. In the present study, the IRI analysis reveals that besides the regions between Rh and Cl as well as between Rh and P, which are typical chemical bonds, the region between Rh and H also displays an attractive intermolecular interaction similar to a hydrogen bond. This intermolecular interaction pre-coordinates the educt to the complex and increases the reaction probability. Due to the lower activation energy and the pre-coordination of Rh and H, the path from I→II is favored over the I'→IV.a channel.

Cl rotation

Beyond the analysis of the C–H addition, we turned our attention to the structure of the five-times coordinated intermediate II. A Localized-orbital Locator (LOL) analysis[26] was performed on complex II, in order to elucidate the electronic nature of the bonds between the central Rh and the various ligands. The three-dimensional LOL function ranges from 0 to 1 and depends on the ratio between the local kinetic energy density and the Kohn-Sham kinetic energy density: The higher the LOL value is, the lower the local kinetic energy of the electrons will be. The cross section defined by the H–Rh-Cl plane of the 3D LOL function is shown in Figure 5b. Alongside the Rh–H bond, a maximum is found close to the H atom. This allows interpreting the bond between Rh and H as a polar covalent bond, as the formation of covalent bonds will lower this local kinetic energy.[27] On the contrary, a region with high local kinetic energy (and thus low LOL value) is visible along the Rh–Cl axis, which leads to the interpretation of an ionic interaction between Rh and Cl. As there exists one remaining vacancy in the five-times coordinated structure, it is possible for ligands to rearrange their positions. Among the five-times coordinated ligands, the chloride ion has the highest flexibility for rearrangement due to the non-directional ionic interaction in the Rh–Cl fragment. The energy change of the chloride rotation is shown in Figure 4b. For most bisphosphine ligands, the conformational change is only slightly endothermic, and the activation energy is relatively low ranging from 4 to 40 kJ mol^{-1}. However, some exceptions could be found for bulky ligands and/or ligands which feature additional halogen atoms in their structure. These halogen atoms have the tendency to interact with the central Rh and, thus, block the vacancy. Therefore, adding on top of the high energy level of species II, the TS associated to the Cl rotation (II→III) could potentially be the TDTS of the entire catalytic cycle, based on the energetic span model, even though the activation barrier of this elementary step itself is not insurmountable.

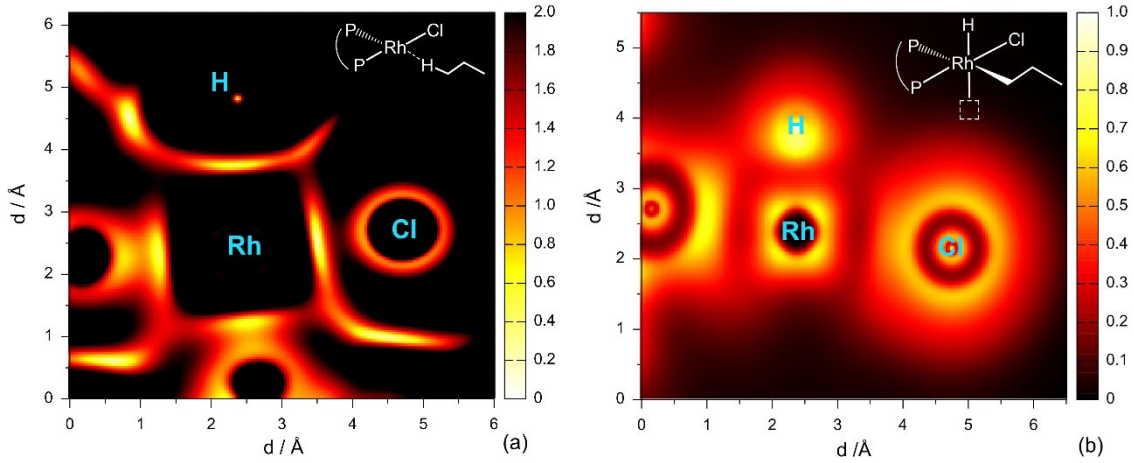

Figure 5. (a) Interaction Region Indicator (IRI) function for visualizing the weak interaction between the Rh and H on propane before addition. (b) Localized-orbital Locator (LOL) function for visualizing different types of chemical bonds in the complex after the oxidative addition. Corresponding Lewis structures are shown in the top-right corner, respectively.

C–C bond formation

Both five-times coordinated Rh(III) species, II and III, display a strong tendency to accept another electron pair, yielding a stable octahedral coordination sphere. Thus, CO insertion into II and III leads to the octahedral structures IV.b and IV.a, respectively, both of which feature an 18-electron configuration. The difference between these two complexes is merely the position of the CO group relative to the bisphosphine ligand: while in IV.a, the CO group is inserted in the equatorial plane defined by P–Rh-P and, thus, trans to one phosphorous, in IV.b, it is in cis position to both phosphorous atoms. Although in both complexes the subsequent C–C formation proceeds via the migration of the propyl group to the CO group, the activation barrier of this reaction step is significantly different depending on the position of the CO ligand. For the path from IV.a to V.a, the activation barrier ranges from 20 to 80 kJ mol^{-1} (Figure 4c represented by filled black dots) depending on the bisphosphine ligands while the activation barrier for the path from IV.b to V.b ranges from 80 to 140 kJ mol^{-1} (represented by hollow triangles in Figure 4c). Thus, the DFT calculations clearly indicate that for most ligands, intermediate IV.b could potentially be a dead end, rendering the path from IV.a to V.a more likely the main reaction pathway. It is important to note that the transformation from IV.a to V.a can only occur after the chloride rotation has taken place (II→III, recall previous subsection), where the TS can be the rate-determining state of the catalytic cycle, depending on the steric demand of the coordinated ligand.

Butyraldehyde generation

After the formation of the new C–C bond and the associated CO insertion, a vacancy in the vicinity of the central Rh ion is formed. This vacancy is filled by another CO molecule to form a stable octahedral, 18-electron complex. The insertion of CO can be achieved via three pathways: *a*) CO directly inserts into the equatorial P–Rh-P plane (V.a→VI.a) after the migration of the propyl group, *b)* from VI.b to V.b, while noteworthy species V.b could not be generated due to the high activation barrier, or *c*) chloride rearrangement from the axial position to the equatorial P–Rh–P plane, followed by the addition of the CO molecule into the axial position (V.a→V.c→VI.c). For all our studied Rh complexes, the formations of both VI.a and VI.c are exothermic, but VI.a is predicted to be the intermediate with the lowest energy (see Section 2 in SI for details). Finally, the product, i. e., butyraldehyde, is obtained by the migration of the carbonyl group to the axial position, accompanied by the rearrangement of the chloride (VI.a→I') taking place in pathway *a)*, or by the rearrangement of CO (VI.c→I') into the equatorial plane in pathway *c)*. As highlighted in Figure 4d, in most cases, the barrier of the carbonyl group migration in pathway *c)* ranges from 20 to 60 kJ mol^{-1} while the respective barrier for pathway *a)* is in general ~80 kJ mol^{-1}. This indicates that VI.a is thermally favored, while the generation of butyraldehyde via path *c)* is kinetically favored. In summary, the computational results indicate that in both cases, the final butyraldehyde product can be obtained, which subsequently recovers the initial species I' closing the catalytic cycle.

Finally, from Figures 4a and c, the strong correlations between driving force and activation barrier of the C–H activation (I→II) and C–C formation (IV.a→V.a) are evident. Therefore, the more stable the five-times coordinated structure (II) is, the lower the activation barrier for the C–H activation is. The same trend is also observed for the C–C formation process. This implies that the energy of TSs can be predicted entirely from the information of the connecting intermediates for step I→II and step IV.a→V.a via linear free-energy relationships based on the Bell–Evans–Polanyi principle.[28] On the other side, the correlation of the TSs and their associated intermediates for the other steps involved in the reaction mechanism is unfortunately not as straightforward. An in-depth study on the utilization of linear free-energy relationships to accelerate the theoretical prediction in the future is currently under way.

Conclusions

Our in-depth computational study unraveled the complete catalytic cycle as well as the leading intermediates involved in the C–H carbonylation of alkanes mediated by bidentate Rh(I)-phosphine complexes. The mechanistic analysis covers details on all key steps, including the C–H oxidative addition, the ligand rearrangement, C–C bond formation and the reductive elimination. It was found that the TS for the initial reaction step, namely C–H activation, is related to the rate-determining state of the catalytic cycle for the vast majority of the investigated Rh catalysts. In addition, it is noteworthy that via the rearrangement of the chloride, the thermodynamics of the reaction can be tuned. Based on our computational results, we predict that the C–H activation step benefits from ligand architectures decorated by multiple phenyl groups or their derivatives – possibly due to conjugation that increases the electron density around the central Rh. On the other hand, decreasing bulkiness of the ligands can reduce the hinderance in the chloride rearrangement. Therefore, a flexible ligand architecture with aromatic rings could potentially increase the performance of Rh-based catalysts.

Furthermore, the activation barriers and the driving forces of several elementary reactions in the cycle show strong correlations, which suggests a great potential for the application of machine learning techniques to partially replace the time-consuming quantum chemical calculations and, thus, to accelerate the ligand screening process. The identified mechanism and its underlying energy landscape will thus serve as a basis for the large-scale screening of new phosphine ligands and the design of the Rh-based catalysts for the C–H activation and subsequent functionalization of alkanes. In a future study, we aim to experimentally solidify the suggested mechanism by in situ spectroscopy studies on the catalytic C–H functionalization of alkanes. The focal point of this upcoming investigation will be the synthesis and application of the best performing ligands from the present study.

Computational Section

All quantum chemical simulations were performed using the Gaussian 16 software package.[29] The [Rh(PLP)(CO)(Cl)] complexes (Figure 1) featuring a bidentate phosphine ligand were investigated to evaluate structure-property relationships with respect to the energy landscape of the catalytic cycle. All these symmetric bisphosphines consist of three main building blocks: The linker L that connects the two chelating phosphorus atoms as well as two different residual groups, R_1 and R_2, located at each phosphorus atom. In this study, we selected a basis of 21 different linkers and 62 residual groups for the initial investigation (see Figure S1 and S2 in SI for details). With the aid of SMILES string representation,[30] the data points in the phosphine-based Rh complex space could be built in a combinatorial manner in a fully automatic fashion. From the resulting ligand space of 38,430 ligands and upon removal of duplicate structures, a set of 20 prototypic ligands was selected to build the respective Rh complexes. The selection process was done in R[31] and its package ChemineR[32] via a k-means clustering analysis. First a 1024-bit long fingerprint was built for each ligand from its respective atom pair library. The fingerprint uses the 1024 most frequent atom pairs found in the atom pair library. Subsequently, the fingerprints were used in a k-means clustering analysis with 10 clusters. From each cluster, two ligands were randomly selected to represent the entire cluster in the following detailed mechanistic analysis.

Closed-shell equilibrium structures, i.e., minima and transition states (TSs) as well as electronic properties of educts, intermediates, and products involved in the C–H activation of propane (methyl group activation) and subsequent steps mediated by the Rh complexes were obtained at the DFT level of theory. The range-separated ωB97XD functional,[33] which was previously successfully applied in the frame of hydrogen formation in structurally related transition metal-based catalysts,[34] [5 + 2] cycloisomerization of ynamide-vinylcyclopropanes catalyzed by Rh-based catalysts[35] and hydrosilylation of C=C and C=O bonds mediated by Rh-complexes[36] was employed. The def2-SVP basis set and the respective effective core potential (ECP) were utilized for all atoms.[37] TSs were fully optimized at the same level of theory using the rational function optimization (RFO) approach[38] as well as nudged elastic band (NEB) method[39] as implemented in the pysisyphus[40] software suite. Subsequently, a vibrational analysis was carried out for each stationary point to verify that a minimum or first-order saddle point was obtained on the 3*N*-6-dimensional potential energy (hyper)surface (PES). The electronic structure, i.e. chemical bond formation and cleavage, was analyzed in-depth using the Localized Orbital Locator (LOL)[26] and the Interaction Region Indicator (IRI)[23] as implemented in Multiwfn.[41] All optimized structures (xyz files) can be found online at the open-source repository of the European Commission *Zenodo* (DOI: 10.5281/zenodo.6865896).

Acknowledgements

T. H. and S. G. gratefully acknowledge funding from Carl-Zeiss-Stiftung "Durchbrüche". R. G. gratefully acknowledges funding from the Joint Bund-Länder Tenure-Track Programm. All calculations were performed at the Universitätsrechenzentrum of the Friedrich Schiller University of Jena. Open Access funding enabled and organized by Projekt DEAL.

Conflict of Interest

The authors declare no conflict of interest.

Data Availability Statement

The data that support the findings of this study are available from the corresponding author upon reasonable request.

Keywords: C–H activation · carbonylation · computational chemistry · reaction mechanisms · rhodium

[1] a) J. G. Speight, *The chemistry and technology of petroleum*, CRC press, **2006**; b) M. W. George, M. B. Hall, O. S. Jina, P. Portius, X.-Z. Sun, M. Towrie, H. Wu, X. Yang, S. D. Zarić, *Proc. Natl. Acad. Sci. USA* **2010**, *107*, 20178–20183.
[2] X. Tang, L. Gan, X. Zhang, Z. Huang, *Sci. Adv.* **2020**, *6*, eabc6688.
[3] D. D. Tanner, G. Lycan, N. Bunce, *Can. J. Chem.* **1970**, *48*, 1492–1497.
[4] a) L. Ackermann, *Chem. Rev.* **2011**, *111*, 1315–1345; b) T. Rogge, N. Kaplaneris, N. Chatani, J. Kim, S. Chang, B. Punji, L. L. Schafer, D. G. Musaev, J. Wencel-Delord, C. A. Roberts, *Nat. Rev. Methods Primers* **2021**, *1*, 1–31.
[5] T. Sakakura, T. Sodeyama, K. Sasaki, K. Wada, M. Tanaka, *J. Am. Chem. Soc.* **1990**, *112*, 7221–7229.
[6] J. A. Leitch, C. G. Frost, *Chem. Soc. Rev.* **2017**, *46*, 7145–7153.
[7] Y. Boutadla, D. L. Davies, S. A. Macgregor, A. I. Poblador-Bahamonde, *Dalton Trans.* **2009**, 5820–5831.
[8] D. L. Davies, S. A. Macgregor, A. I. Poblador-Bahamonde, *Dalton Trans.* **2010**, *39*, 10520–10527.
[9] a) H. Cheung, R. S. Tanke, G. P. Torrence, in *Ullmann's Encyclopedia of Industrial Chemistry* **2000**; b) J. Guan, A. Wriglesworth, X. Z. Sun, E. N. Brothers, S. D. Zarić, M. E. Evans, W. D. Jones, M. Towrie, M. B. Hall, M. W. George, *J. Am. Chem. Soc.* **2018**, *140*, 1842–1854.
[10] a) T. R. Kégl, N. Pálinkás, L. Kollár, T. Kégl, *Molecules* **2018**, *23*, 3176; b) C. A. Tolman, *J. Am. Chem. Soc.* **1970**, *92*, 2953–2956.
[11] W. A. Herrmann, *Angew. Chem. Int. Ed.* **2002**, *41*, 1290–1309; *Angew. Chem.* **2002**, *114*, 1342–1363.
[12] Q. Teng, H. V. Huynh, *Inorg. Chem.* **2014**, *53*, 10964–10973.
[13] T. Gensch, M. Hopkinson, F. Glorius, J. Wencel-Delord, *Chem. Soc. Rev.* **2016**, *45*, 2900–2936.
[14] S. Kawamorita, T. Miyazaki, H. Ohmiya, T. Iwai, M. Sawamura, *J. Am. Chem. Soc.* **2011**, *133*, 19310–19313.
[15] S. P. Semproni, C. C. H. Atienza, P. J. Chirik, *Chem. Sci.* **2014**, *5*, 1956–1960.
[16] G. Schwarzenbach, *Helv. Chim. Acta* **1952**, *35*, 2344–2359.
[17] a) R. J. Lundgren, M. Stradiotto, in *Key Concepts in Ligand Design: An Introduction*, Wiley: West Sussex, England, **2016**; b) W. A. Munzeiwa, B. Omondi, V. O. Nyamori, *Beilstein J. Org. Chem.* **2020**, *16*, 362–383.
[18] a) S. E. Bromberg, T. Lian, R. G. Bergman, C. B. Harris, *J. Am. Chem. Soc.* **1996**, *118*, 2069–2072; b) D. P. Drolet, A. J. Lees, *J. Am. Chem. Soc.* **1992**, *114*, 4186–4194.
[19] J. S. Bridgewater, T. L. Netzel, J. R. Schoonover, S. M. Massick, P. C. Ford, *Inorg. Chem.* **2001**, *40*, 1466–1476.
[20] E. P. Wasserman, C. B. Moore, R. G. Bergman, *Science* **1992**, *255*, 315–318.
[21] H. Yang, K. T. Kotz, M. C. Asplund, M. J. Wilkens, C. B. Harris, *Acc. Chem. Res.* **1999**, *32*, 551–560.
[22] a) S. Kozuch, S. Shaik, *Acc. Chem. Res.* **2011**, *44*, 101–110; b) S. Kozuch, *Wiley Interdiscip. Rev.: Comput. Mol. Sci.* **2012**, *2*, 795–815.
[23] T. Lu, Q. Chen, *Chem. Methods* **2021**, *1*, 231–239.
[24] E. R. Johnson, S. Keinan, P. Mori-Sánchez, J. Contreras-García, A. J. Cohen, W. Yang, *J. Am. Chem. Soc.* **2010**, *132*, 6498–6506.
[25] J. Contreras-García, E. R. Johnson, S. Keinan, R. Chaudret, J.-P. Piquemal, D. N. Beratan, W. Yang, *J. Chem. Theory Comput.* **2011**, *7*, 625–632.
[26] H. Schmider, A. Becke, *J. Mol. Struct.* **2000**, *527*, 51–61.
[27] R. Bader, *Atoms in molecules: a quantum theory*, Oxford University Press, USA, **1994**.

[28] a) M. Evans, M. Polanyi, *Trans. Faraday Soc.* **1938**, *34*, 11–24; b) W. P. Jencks, *Chem. Rev.* **1985**, *85*, 511–527.
[29] M. J. Frisch, G. W. Trucks, H. B. Schlegel, G. E. Scuseria, M. A. Robb, J. R. Cheeseman, G. Scalmani, V. Barone, G. A. Petersson, H. Nakatsuji, X. Li, M. Caricato, A. V. Marenich, J. Bloino, B. G. Janesko, R. Gomperts, B. Mennucci, H. P. Hratchian, J. V. Ortiz, A. F. Izmaylov, J. L. Sonnenberg, Williams, F. Ding, F. Lipparini, F. Egidi, J. Goings, B. Peng, A. Petrone, T. Henderson, D. Ranasinghe, V. G. Zakrzewski, J. Gao, N. Rega, G. Zheng, W. Liang, M. Hada, M. Ehara, K. Toyota, R. Fukuda, J. Hasegawa, M. Ishida, T. Nakajima, Y. Honda, O. Kitao, H. Nakai, T. Vreven, K. Throssell, J. A. Montgomery Jr., J. E. Peralta, F. Ogliaro, M. J. Bearpark, J. J. Heyd, E. N. Brothers, K. N. Kudin, V. N. Staroverov, T. A. Keith, R. Kobayashi, J. Normand, K. Raghavachari, A. P. Rendell, J. C. Burant, S. S. Iyengar, J. Tomasi, M. Cossi, J. M. Millam, M. Klene, C. Adamo, R. Cammi, J. W. Ochterski, R. L. Martin, K. Morokuma, O. Farkas, J. B. Foresman, D. J. Fox, Wallingford, CT, **2016**.
[30] D. Weininger, *J. Chem. Inf. Model.* **1988**, *28*, 31–36.
[31] R Core Team, "R: A language and environment for statistical computing", R Foundation for Statistical Computing, Vienna, Austria, **2013**, URL http://www.R-project.org/.
[32] Y. Cao, A. Charisi, L.-C. Cheng, T. Jiang, T. Girke, *Bioinformatics* **2008**, *24*, 1733–1734.
[33] J.-D. Chai, M. Head-Gordon, *Phys. Chem. Chem. Phys.* **2008**, *10*, 6615–6620.
[34] S. Bandaru, N. J. English, A. D. Phillips, J. MacElroy, *Catalysts* **2017**, *7*, 140.
[35] R. Straker, Q. Peng, A. Mekareeya, R. Paton, E. Anderson, *Nat. Commun.* **2016**, *7*, 1–9.
[36] L. Zhao, N. Nakatani, Y. Sunada, H. Nagashima, J.-y. Hasegawa, *J. Org. Chem.* **2019**, *84*, 8552–8561.
[37] F. Weigend, R. Ahlrichs, *Phys. Chem. Chem. Phys.* **2005**, *7*, 3297–3305.
[38] J. Simons, P. Joergensen, H. Taylor, J. Ozment, *J. Phys. Chem.* **1983**, *87*, 2745–2753.
[39] H. Jónsson, G. Mills, K. W. Jacobsen, in *Classical and Quantum Dynamics in Condensed Phase Simulations* (Eds.: B. J. Berne, G. Ciccotti, D. F. Coker), World Scientific, Singapore, **1998**, pp. 385–404.
[40] J. Steinmetzer, S. Kupfer, S. Gräfe, *Int. J. Quantum Chem.* **2021**, *121*, e26390.
[41] T. Lu, F. Chen, *J. Comput. Chem.* **2012**, *33*, 580–592.

Manuscript received: July 6, 2022
Revised manuscript received: July 21, 2022
Accepted manuscript online: July 22, 2022
Version of record online: August 18, 2022